Reorganization of Retinotopic Maps after Occipital Lobe Infarction

Lucia M. Vaina[1,2,3], Sergei Soloviev[3], Finnegan J. Calabro[3], Ferdinando Buonanno[1,2,3], Richard Passingham[4], and Alan Cowey[3,4*]

Abstract

■ We studied patient JS, who had a right occipital infarct that encroached on visual areas V1, V2v, and VP. When tested psychophysically, he was very impaired at detecting the direction of motion in random dot displays where a variable proportion of dots moving in one direction (signal) were embedded in masking motion noise (noise dots). The impairment on this motion coherence task was especially marked when the display was presented to the upper left (affected) visual quadrant, contralateral to his lesion. However, with extensive training, by 11 months his threshold fell to the level of healthy participants. Training on the motion coherence task generalized to another motion task, the motion discontinuity task, on which he had to detect the presence of an edge that was defined by the difference in the direction of the coherently moving dots (signal) within the display. He was much better at this task at 8 than 3 months, and this improvement was associated with an increase in the activation of the human MT complex (hMT^+) and in the kinetic occipital region as shown by repeated fMRI scans. We also used fMRI to perform retinotopic mapping at 3, 8, and 11 months after the infarct. We quantified the retinotopy and areal shifts by measuring the distances between the center of mass of functionally defined areas, computed in spherical surface-based coordinates. The functionally defined retinotopic areas V1, V2v, V2d, and VP were initially smaller in the lesioned right hemisphere, but they increased in size between 3 and 11 months. This change was not found in the normal, left hemisphere of the patient or in either hemispheres of the healthy control participants. We were interested in whether practice on the motion coherence task promoted the changes in the retinotopic maps. We compared the results for patient JS with those from another patient (PF) who had a comparable lesion but had not been given such practice. We found similar changes in the maps in the lesioned hemisphere of PF. However, PF was only scanned at 3 and 7 months, and the biggest shifts in patient JS were found between 8 and 11 months. Thus, it is important to carry out a prospective study with a trained and untrained group so as to determine whether the patterns of reorganization that we have observed can be further promoted by training. ■

INTRODUCTION

People can recover remarkably well from the effects of cortical lesions. This is best demonstrated in the case of lesions that involve either sensory or motor areas. Physiological techniques can be used to identify and then map the damaged region. The same techniques can then be used to chart whether after the damage there are changes in the mapping over time.

There is an added advantage in working with a sensory system, because sensory thresholds provide an objective measure of improvement. For example, the threshold for discriminating the direction of motion can be measured as the minimum number of dots that have to move coherently for motion to be detected. Vaina, Cowey, Eskew, LeMay, and Kemper (2001) showed that, if patients with unilateral lesions of the human MT complex (hMT^+) are tested repeatedly, some could regain normal thresholds, even when the displays are presented to the affected hemisphere. Huxlin et al. (2009) reported that similar recovery could be found after large lesions of V1. Moore, Rodman, and Gross (2001) made striate lesions in monkeys and reported that they could detect the direction of coherent motion so long as the displays were large. However, in this case, the lesions were made soon after birth, whereas in the study by Huxlin et al., the patients suffered lesions as adults.

One possibility that could explain these results is that improvement can occur because of changes in the sensory maps. These maps have turned out to be surprisingly plastic. We distinguish three situations. For all three, there are supporting data from experiments in cats and monkeys.

The first involves changes that occur in primary sensory maps after the peripheral input to part of the map is cut off. For example, remapping can occur in area S1 after the loss of a digit (Merzenich et al., 1984) or section of

[1]Massachusetts General Hospital, [2]Harvard Medical School, [3]Boston University, [4]University of Oxford
*Deceased December 2012.

Journal of Cognitive Neuroscience 26:6, pp. 1266–1282
doi:10.1162/jocn_a_00538

the dorsal column (Jain, Qi, Collins, & Kaas, 2008) and in V1 after a retinal lesion (Chino, 1995). The finding is that, over time, neurons in the deafferented part of the map can become responsive to stimulation of the adjacent tissue. If the lesion is complete, as in the loss of a digit or section of the dorsal column, it is stimulation of the neighboring digit (Merzenich et al., 1984) or face (Jain et al., 2008) that evokes responses. If the lesion is incomplete, as in the case of small retinal lesions, it is stimulation of the retina adjacent to the lesion that does so (Chino, 1995).

In these cases, cell activity is weak at first (Chen, Qi, & Kaas, 2012), and it is not yet clear to what extent it can become normal over time. Chino (1995) recorded from neurons and claimed that 3 months after a bilateral retinal lesion the responses were relatively normal so long as the stimuli were high contrast. Smirnakis et al. (2005) queried this claim and reported that V1 did not regain normal responsivity either when measured with fMRI or with multiunit recording. It is unlikely that the difference in these studies would be because of the use of fMRI as suggested by Calford et al. (2005) because Chen et al. (2012) found fMRI to be sensitive to subthreshold activity.

These studies recorded activity within 3 months of the lesion, and studies are needed to track the responsiveness of neurons over a longer time period. Early changes may be because of unmasking of latent inputs because of a loss of GABA (Garraghty & Kaas, 1991), but there are also later changes in AMPA receptors (Garraghty, Arnold, Wellman, & Mowery, 2006) and in the morphology of the dendrites of neurons in the affected area (Churchill, Tharp, Wellman, Sengelaub, & Garraghty, 2004).

The second situation involves a lesion in part of the cortical map itself. Here there is no possibility that responsiveness could be regained within the lesioned area itself. However, after a partial lesion of V1, it is possible to record an increase in activity over time in the area adjacent to the lesion (Eysel, 2009). After some time, there is an increase in the size of the receptive fields of the neurons in the adjacent tissue. Possible mechanisms include a change in *N*-methyl-D-aspartate receptor function (Yan et al., 2012).

The third situation involves changes of activity in higher cortical sensory areas when they are deprived of part of their input by a lesion in earlier sensory areas. The result can depend on the stimulus used. For example, after a lesion in V1, neurons in MT still respond to the direction of moving bars (Rodman, Gross, & Albright, 1989), but they no longer respond to the direction in random dot kinematogram (RDK) displays (Azzopardi & Cowey, 2001). However, there is evidence that neurons adjacent to the region of MT that has lost its retinotopic input may show changes in their receptive fields and the deprived part of MT may regain a limited ability to respond to stimulation of the intact part of V1 (Collins, Lyon, & Kaas, 2003).

These findings raise three questions relating to the recovery of performance on a motion task that can occur in patients with cortical lesions (Vaina et al., 2001). The first is whether changes of the sort reported in animals can be found in patients with lesions in early cortical sensory areas. We had the opportunity to study a patient (JS) with a localized unilateral infarct that involved the upper quadrant of V1 to V2v and VP. The patient was tested on his ability to discriminate the direction of motion in RDK displays where a variable proportion of dots provided motion signal (direction) whereas the others provided masking motion noise. When the displays were presented to the affected quadrant, he was extremely impaired at first, but with repeated testing over an 11-month period, his threshold improved to a normal or better-than-normal level. In the quadrant corresponding to the normal hemisphere, he was also somewhat impaired at first, but his performance became normal at 3 months after the lesion (see Figure 2A later in this article).

We scanned this patient with fMRI at 3, 8, and 11 months postinfarct and mapped the early visual areas in the occipital lobes to see if there were changes in his retinotopy and area hMT^+ that was not involved in his lesion but is involved in processing the visual motion stimulus he was trained on. We also looked at his visual retinotopic map, not only for changes in size of retinotopic areas but also for displacement, because shifts have been reported after cortical dysgenesis (Slotnick, Moo, Krauss, & Hart, 2002). We scanned repeatedly because of suggestions in the animal literature that changes in mapping after deafferentation can occur progressively and over a similar time period (Churchill, Muja, Myers, Besheer, & Garraghty, 1998). We were thus able to see whether changes also occur after a cortical lesion in humans. We also scanned three healthy controls who were trained on the same motion task as patient JS to check whether similar changes could be detected in the absence of a lesion.

The second question is what effect any changes in retinotopic organization have on processing in higher visual areas that are involved in detecting direction in motion coherence stimuli, even if these areas are not involved in the lesion. We localized hMT^+ by scanning while the participants performed a motion coherence task. We also measured behavioral improvement on two such tasks in patient JS and repeated scans so as to see if we could relate that improvement to changes in activation in hMT^+.

The final question is whether the changes occur spontaneously or whether they can be promoted by formal training. Eysel (2009) reported that repeated visual stimulation could induce more rapid change in the receptive fields after a visual cortical lesion. We addressed this question retrospectively in a patient (PF) that we had studied and who had a comparable lesion. Patient PF had a left occipital lobe infarct in V1 that extended significantly into V2v, the upper right quadrant of his visual field. This patient had not been involved in retraining on the motion coherence task or any other task. He had been scanned at 3 and 7 months. We were thus able to see whether there were changes in the retinotopic areas that were

comparable with those seen in the first two scans obtained on patient JS.

METHODS

Participants

We studied seven right-handed men between 23 and 42 years old. Two were patients who had had single strokes, and the other five were healthy controls. All were alert, cooperative, and good at maintaining fixation on the psychophysical studies. All had normal or corrected-to-normal visual acuity.

Patient JS (25 years old) had a unilateral occipital infarct in the right hemisphere, and patient PF (42 years old) had had a unilateral occipital infarct in the left hemisphere (Figure 1A, B).

Both patients had an upper quadrantanopia in the visual field contralateral to the lesion. The lesion in patient JS lesion affected the right occipital cortex in the lingual gyrus and cuneus (Figure 1A); the lesion in patient PF produced cortical damage in the left lingual gyrus (Figure 1B). The infarct was caused in these patients by inadequate closure of the atrial septum in the heart (patent foramena ovale); this was their only medically relevant problem.

After the infarct, the patients underwent complete neuro-ophthalmological evaluations, including visual field tests using automated Humphrey perimetry, repeated twice and performed by the same technician (see Figure 1C, D). The patients complained of difficulties with several aspects of visual perception including visual motion. On formal testing with a subset of our motion stimuli, JS and PF were initially impaired on discrimination of direction and motion discontinuity tested with RDK displays where a variable proportion of the dots provided directional information, that is, signal, whereas the rest were nondirectional and so constituted noise (Vaina et al., 2001; Vaina, LeMay, Bienfang, Choi, & Nakayama, 1990; Newsome & Paré, 1988).

All procedures were carried out in accordance with the Declaration of Helsinki and were approved by the institutional review boards of Boston University and Athinoula Martinos Center for Biomedical Imaging, Massachusetts General Hospital, Harvard University. The participants were informed of the psychophysical and fMRI procedures, and written informed consent was obtained.

Stimulus and Experimental Methods

Psychophysics

RDK stimuli were generated using the C programming language in conjunction with the Video toolbox (Pelli, 1997) and MacGLib 2.0 (Micro ML Inc., Québec, Canada) programming libraries and were displayed with an Apple computer and 18-in. Apple CRT. The stimuli were adapted from Vaina et al. (1990, 2001) and Newsome and Paré (1988). They were RDKs composed of randomly positioned dots (6 arcmin in diameter; with a density of 2 dots/deg^2) displayed in an imaginary circle of gray background and having a correlated motion signal of variable strength embedded in masking motion noise (Figure 2B). The dots were high-contrast black on a medium gray background to avoid the confound of light scatter. Dots that traveled

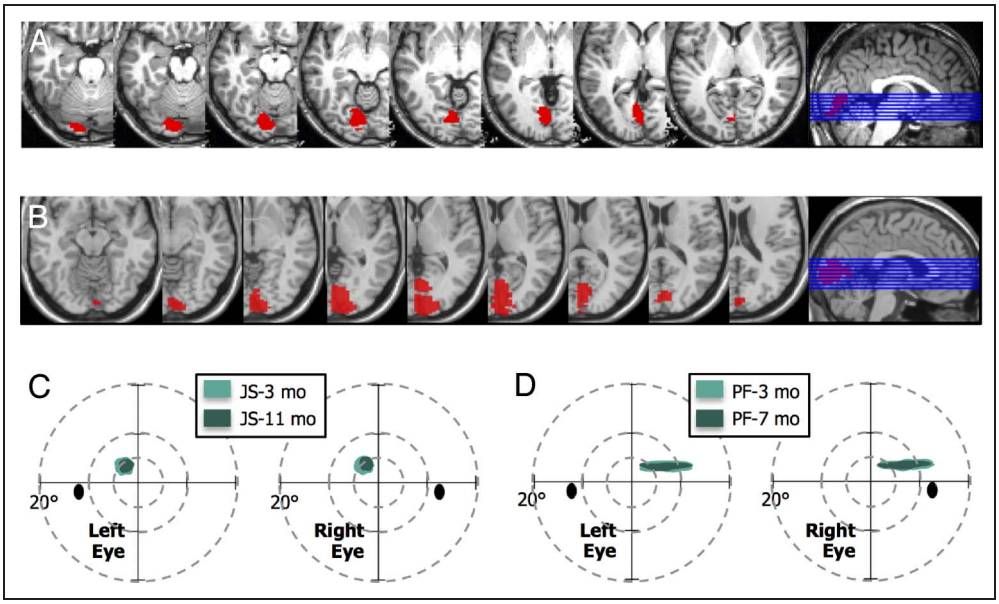

Figure 1. Lesion localization and visual field maps for patients JS and PF. (A, B) Axial slices of the T2 weighted image obtained in structural magnetic resonance scans (Siemens 3T) showing lesion locations, with a sagittal view indicating the positions of the slices, for (A) JS and (B) PF. The right hemisphere infarction of patient JS involved part of the primary visual cortex and the immediately adjacent extrastriate areas. Patient's PF infarct involving part of the primary visual cortex and immediately surrounding extrastriate areas in the left occipital lobe and minimally extending in the adjacent medial-temporal lobe. (C, D) Schematic of Humphrey automated perimetry for mapping visual field loss. Perimetry in patient JS was obtained at 3 and 9.5 months after the lesion and showed a paracentral upper left scotoma, initially 5° in diameter with the dense part of the scotoma reduced to 3.5° diameter at the later assessment. The field loss corresponded to a reduction in the cortical representation of the visual field. Perimetry of patient PF showed a stable visual field loss in the upper right quadrant at 3 and 7 months poststroke. Only the dense part of the scotoma is shown in both patients.

outside the circular aperture were replotted at the opposite edge of the aperture to keep dot density constant.

Contrast, mean luminance, and spatial and temporal frequency content did not change in the RDK stimuli. The speed of motion was 3°/sec, defined as the distance a signal dot was displaced between successive frames. These types of displays have been used for more than 20 years in our laboratory in several psychophysical motion tasks both with healthy participants and stroke patients and have also been used extensively in experiments designed to localize hMT^+ with fMRI.

Motion Coherence

RDKs were presented within a 6° imaginary aperture with the properties described above. A variable proportion of the dots constituted the signal, moving coherently in one of the cardinal directions (up, down, left, or right); the remainder dots were repositioned between frames to provide masking motion noise. Signal dots were chosen independently on each frame so that individual dots could not be tracked to determine direction, because it was unknown which dots would be signal on any given frame. The stimuli were presented 2° off the border of the horizontal and vertical meridians so as to fall on a preselected location in the upper left (affected) or upper right (unaffected) visual field quadrant. Fixation was at the center of the screen. We used an adaptive staircase procedure (Vaina et al., 2003) to determine the percentage of signal dots necessary to determine response threshold. The participants' task was to determine in a four-alternative forced-choice (4AFC) whether the global direction of the RDK appeared to be up, down, left, or right. A schematic of the stimulus is shown in Figure 2B. The participants were asked to respond as soon as possible and as accurately as possible.

Motion Discontinuity

An RDK with the properties described above was displayed in a 6° circular aperture. Identical to the motion coherence task, the stimuli were presented 2° off the border of the horizontal and vertical meridians so as to fall on a preselected location in the upper left (affected) or upper right (unaffected) visual field quadrant. Fixation was at the center of the screen. In a yes/no detection task, participants were asked to determine whether the display was homogeneous as in the motion coherence test (MCT; in this condition, all the signal dots moved in the same direction, up or down) or if it had an illusory edge (a discontinuity) passing through the center of the display. This discontinuity was defined by the difference in direction of the signal dots, with half of the display signal dots moving upward and the other half moving downward. The illusory edge was randomly chosen to be horizontal, vertical, or diagonal. A schematic of the test stimuli is shown in Figure 3B. The participants were asked to respond as soon and as accurately as possible whether the display was homogeneous (the signal dots moved in the same direction) or whether it contained a discontinuity.

Behavioral Training

Patient JS was trained on the MCT described above, for 8 months, twice weekly, for 300 trials each time. Because we were interested to determine whether improvement occurred for stimuli presented in the quadrant with the scotoma, the stimuli were presented 2° off the border of the horizontal and vertical meridians so as to fall on a preselected location in the upper left (affected) or upper right (unaffected) visual field quadrant. Fixation was at the center of the screen. In each training session, two thresholds were obtained on the MCT, and these were averaged to determine the coherence level for training. During training, which was done using constant stimuli, at three coherence levels, trials were presented in a randomized sequence at each of three coherence levels defined as threshold and threshold plus or minus one standard deviation. Toward the end of training, when the performance of JS improved significantly (Figure 2C, top), the threshold coherence or standard deviations were too small for using the definition of the constant stimuli described above. We used threshold and plus/minus 4–5% coherence levels. No feedback was ever given as to the correctness of the response.

MRI and fMRI Scanning

Schedule of Scans

The fMRI scans were repeated approximately 6 months apart in three of the healthy controls and in the two patients. Patient JS was scanned three times at 3, 8, and 11 months after the infarct, and patient PF was scanned twice, at 3 and 7 months after the infarct. Controls and both patients underwent retinotopic mapping (as described below) in each scan.

Patient JS performed the motion coherence task (with central fixation) in all three of the fMRI scans, and the motion discontinuity task in the first two of the fMRI scans. We focused on area hMT^+ because many laboratories, including ours, have shown to be selectively activated on tasks that involve motion coherence stimuli (e.g., Braddick et al., 2001; Vaina et al., 1990, 2001; Morrone et al., 2000). In the motion discontinuity task, in addition to the area hMT^+, we also focused on the lateral occipital area kinetic occipital region (KO) or V3B known to be involved in extracting edges that are defined by difference in motion (Dupont et al., 1997; Van Oostende, Sunaert, Van Hecke, Marchal, & Orban, 1997) and also in the analysis of optic flow (Vaina et al., 2010; Greenlee, 2000; Rutschmann, Schrauf, & Greenlee, 2000).

Image Acquisition

All imaging was done at the Martinos Center for Biomedical Imaging, Massachusetts General Hospital on a 3.0-T Siemens Trio high-speed EPI device (Siemens Ltd., Enlargen, Germany) with a quadrature head coil. During scanning participants were fitted with earplugs. They lay supine within the bore of the magnet with a forehead strap and foam pads placed tightly around the ears and head to minimize head motion. Head motion was detected and corrected using the Martinos Center's automatic image registration algorithm (Woods, Cherry, & Mazziotta, 1992).

In both patients and healthy control, we obtained two conventional high-resolution 3-D T1 weighted MPRAGE anatomical images for 6.5 min each. There were 1-mm isotropic voxels, with a repetition time (TR) of 2530 msec, an echo time (TE) of 3.49 msec, and a flip angle of 7°. The anatomical scans were used for cortical surface reconstruction and for registering the functional scans to the participant's anatomy. In the two patients, we also acquired a high-resolution isotropic (1 mm) set of T2-Space MRI images for lesion localization with a TR of 3200 msec and a TE of 839 msec. All structural images are obtained in NIFTI format, which were used with MRIcron (www.sph.sc.edu/comd/rorden/mricron/) for lesion visualization. The fMRI data were analyzed and visualized using MEDx, FS-Fast, and Freesurfer.

Special gradient-echo EPI sequences (Siemens' PACE sequences), which follow closely the motion of the head, were used to reduce head motion artifacts and scanner drift. The Siemens autoalign protocol developed by van der Kouve at the Martino's Center was used in each fMRI scanning to assure the registration of the imaged slices to the location of a predetermined brain template (www.nmr.mgh.harvard.edu/~andre/Autoalign/Autoalign-instructions.html). This guarantees that a participant will be scanned at the same slice positions in every run and every new scanning session. A field shimming procedure was used to minimize magnetic susceptibility distortions (Reese, Davis, & Weisskoff, 1995).

Whole-brain fMRIs were acquired using gradient EPI sequences for measurement of BOLD signals In patient JS and controls, the functional BOLD image volume constituted 22 contiguous 5-mm-thick slices with a 1-mm gap and a field of view of 20 × 20 cm. The TR was 2.5 sec, and the TE was 70 msec, with a flip angle of 90°. In patient PF, the functional BOLD image volume consisted of 33 contiguous 3.6-mm-thick slices with no gap and field of view of 20 × 20 cm. The TR was 2 sec, and the TE was 30 msec, with a flip angle of 90°.

Analysis of fMRI Data on the Behavioral (Motion) Tasks

During fMRI, the motion coherence stimulus had the same properties as the stimulus used in the behavioral task described above, except here its diameter subtended 12° and it was presented in the central visual field and with central fixation. As in the psychophysical testing and training, in fMRI was also a 4AFC task, with participants instructed to report the direction of global motion. In the stimulus periods, the strength of the motion signal was determined by the proportion of correlated dots or signal dots that were displaced between frames by a fixed spatial offset in one of four cardinal directions, up, down, left, and up. The remaining dots (noise dots) were positioned randomly within the stimulus aperture.

The motion discontinuity test (MDT) used in fMRI was identical to the one administered during psychophysical testing. During scanning, the stimulus was placed in the upper ipsilesional or upper contralesional quadrant, with its edge positioned 2° off the vertical and horizontal meridians. The stimulus location, that is the quadrant of presentation, was counterbalanced across six runs.

In the two psychophysical tasks, we used a blocked design paradigm consisting of eight 20-sec OFF periods (baseline) and seven 20-sec ON periods, interleaved. The ON period consisted of a series of motion coherence or motion discontinuity stimuli displayed through constant stimuli (with coherence levels chosen as in the behavioral task, at threshold, threshold − *SD*, and threshold + *SD*), whereas the OFF period contained directionally randomized noise dots that were otherwise matched to all the stimulus properties (density, size, luminance, speed). Each run started and ended with the presentation of the baseline (OFF period). Motion coherence and motion discontinuity runs were interleaved in a pseudorandom sequence.

No spatial or temporal smoothing was performed on the data. The functional data on the behavioral tasks in patient JS were analyzed using the MEDx 3.4.2 software package (Sensor Systems, Sterling, VA), and additional scripts were developed in our laboratory in MATLAB and Perl. The initial steps of the analysis followed our previously published methods (Vaina & Soloviev, 2004; Vaina et al., 2001). Briefly, active brain regions were determined by means of a *t*-test comparison of activation during the ON and OFF periods of the experimental paradigm. Because of hemodynamic response delay, increased blood flow remains for about 4–8 sec after the task (Friston, Jezzard, & Turner, 1994), so we shifted the analysis blocks by 5 sec relative to the stimulus timing (so that each ON period was defined to start 5 sec after the stimulus started and ended 5 sec after the stimulus completed). The first four TRs were discarded to eliminate nonequilibrium effects. A statistical significance threshold of $p < .05$ (resel corrected) was applied to the data with an extent threshold of a minimum cluster size of five voxels (Worsley et al., 1996; Worsley, Evans, Marrett, & Neelin, 1992). For each participant, EPI images were registered to the high-resolution deskulled structural volume. The same transformation was applied to the statistical data. Thresholded statistical maps were superimposed onto a high-resolution

structural volume. Activation area was computed by multiplying the number of active voxels by the size (in mm^3) of each voxel.

To localize area hMT^+, we aligned the activation on the motion coherence task with the high-resolution structural brain volume. Localization was done by comparing activations evoked by the task period with the baseline period and by the invariant anatomical position of hMT^+ at the junction of the ascending limb of the inferior temporal sulcus and the lateral occipital sulcus (Dumoulin et al., 2000). The results were consistent with the automated anatomical labeling of cortical structures provided by Free Surfer (Fischl et al., 2004). Similar to the other ROIs' areas, in each scan the size of the hMT^+ area was computed by multiplying the number of active voxels ($Z > 3$) inside the ROI by the volume of the voxel.

Lesion Localization

In both patients, we used the MRIcron software package (www.sph.sc.edu/comd/rorden/mricron) to localize and visualize the lesions. Lesions were drawn manually on axial slices, and the brains were transformed to MNI space (Montreal Neurological Institute). Axial slice views of the lesions are shown in Figure 1A and B, with slices chosen to span the extent of the lesions (z coordinates of -9 to $+18$ in JS and -16 to $+8$ in PF). Their location in the occipital lobes is illustrated on a sagittal slice for each patient in the last panel in Figure 1A and B.

The lesion in patient JS was in the right hemisphere. It was subtotal in V1, and it extended into the ventral visual stream, including V2v and VP as seen from the retinotopic mapping and the structural MRI scan. The lesion in patient PF was in the left hemisphere. It was also subtotal in V1, but it included almost all of V2v in the ventral visual stream as shown by retinotopic functional mapping and by the structural MRI scan.

Retinotopic Mapping

Retinotopic mapping was carried out three times in patient JS and twice in patient PF following established procedures (Wandell, Dumoulin, & Brewer, 2007; Wandell, 1999; Tootell, Mendola, Hadjikhani, Liu, & Dale, 1998; Engel et al., 1994). Briefly, the retinotopic mapping stimuli, adapted from (Wandell, 1999), consisted of high-contrast, flickering (2 Hz) checkerboards, moving either as a rotating wedge or expanding ring (Engel, Glover, & Wandell, 1997). The stimuli moved in a periodic pattern and completed a full cycle in 40 sec with a total of seven cycles per scanning run. Each run lasted for 285 sec, where the first four TRs were discarded to eliminate nonequilibrium effects. Each stimulus location was shown for 5 sec, and there were eight locations in a cycle. The wedge subtended 45°, and the rings were 1/8 of the maximum stimulus radius (approximately 1.75° width). The full field of view of the stimulus set (wedges and expanding rings) was 14° of visual angle. Fixation was controlled by having the participant monitor a fixation point (filled red circle) and report an occasional and unpredictable change in color.

The data for patient JS were analyzed using the 3-D phase-encoded retinotopic mapping technique of Dumoulin et al. (2003). This has the advantage that it does not require the reconstruction of the cortical surface. In this method, the visual field sign identification is completely automatic and the method directly supplies volumes for an ROI analysis. The power spectrum of each voxel's time series was computed by a discrete Fourier transform and used in the construction of two phase maps. One map was created by taking the phase of the fundamental frequency varied as a function of polar angle when the stimulus was the rotating wedge and the other by taking the phase of the fundamental frequency varied as a function of eccentricity when stimulus was expending rings. The t-statistical maps were created using a Spearman rank order test for each voxel, with the phase taken from the corresponding phase map.

To calculate the field sign map, three partial derivative maps were used, for polar angle, eccentricity, and cortex. These were computed by convolving the volumes with the partial derivative of a Gaussian kernel. The partial derivative map identifies the cortical surface normals. The visual sign map (VFS) was multiplied by the t-statistical map to create a weighted map of the visual field sign computation (tVFS). The absolute values in the resulting maps indicate a statistical certainty of the visual field sign computation (Dumoulin et al., 2003). Retinotopic areas were identified in the tVFS map by manually outlining and labeling retinotopic areas on the reconstructed brain surface and the tVFS map, starting with area V1, centered around the calcarine sulcus and having negative field sign, and extending both ventrally and dorsally into the higher areas.

To estimate the volume of a retinotopic ROI, we multiplied the number of voxels inside the ROI by the volume of the voxel. We further computed the surface-based coordinates using routines from Free Surfer (https://surfer.nmr.mgh.harvard.edu). Specifically, the retinotopic ROIs were manually labeled on a 2-D flat map using FreeSurfer, where each ROI consisted of a set of the nearest nodes on a mesh describing the boundary of the white–gray matter interface. Mesh nodes are the vertices of the triangular patches that form 3-D cortical manifold obtained in brain surface reconstruction. The area of an ROI is simply the sum of the area of each of triangles (Fischl, Liu, & Dale, 2001; Dale, Fischl, & Sereno, 1999; Fischl, Sereno, & Dale, 1999).

Retinotopic mapping was also obtained on patient PF. As explained in the introduction, this patient was chosen retrospectively to see whether changes in retinotopic organization could also be observed after the lesion in absence of formal training on visual tasks. In patient PF, retinotopic analysis had been performed using the standard techniques incorporated in Freesurfer (Engel et al., 1994, 1997; DeYoe et al., 1996; Sereno et al., 1995).

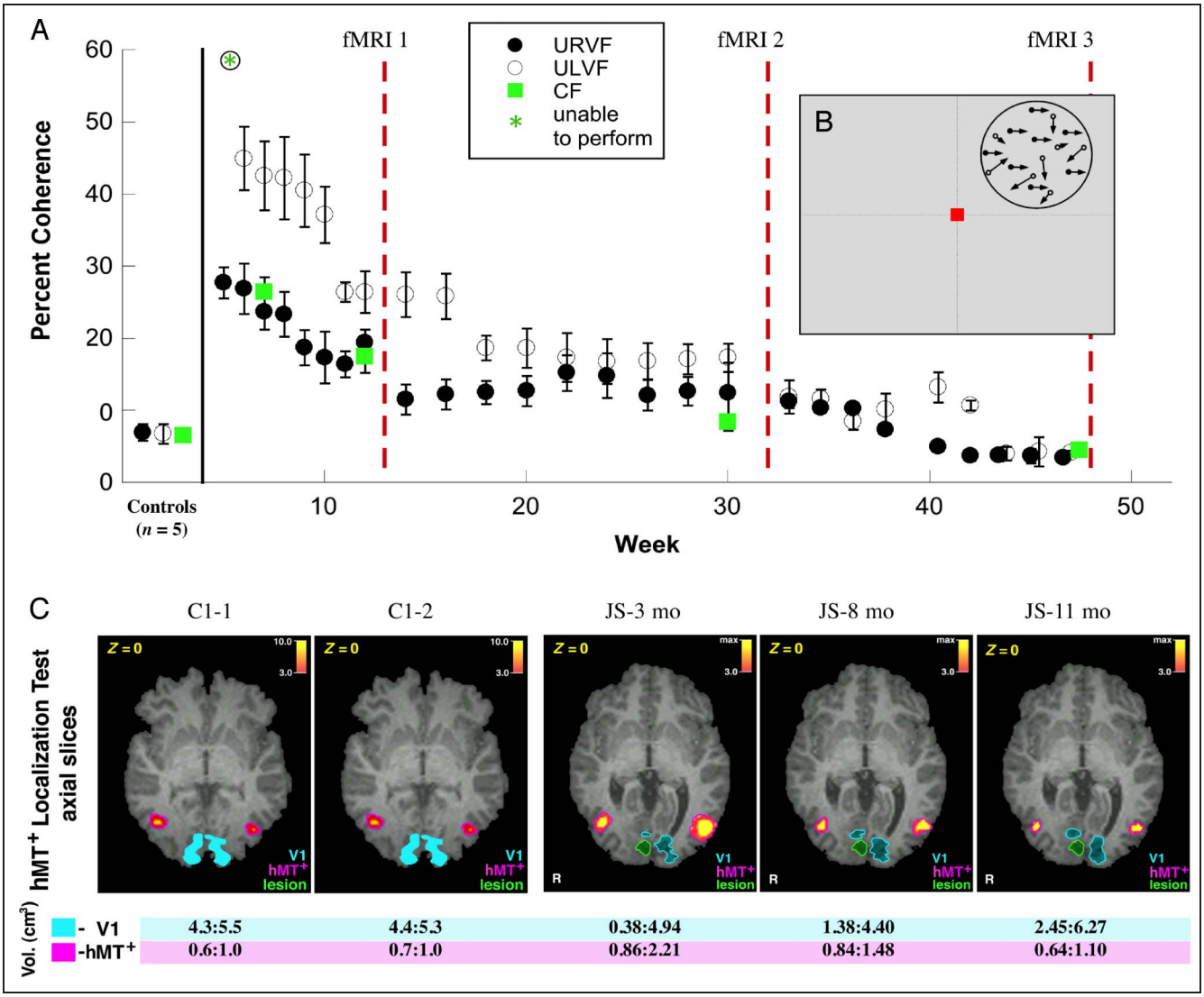

Figure 2. Learning motion coherence. (A) Performance of patient JS on the motion coherence task during training between 3 and 11 months following his stroke. The symbols (open and filled circles) show mean coherence thresholds (the proportion of signal dots necessary to perform the task) from staircases collected at the beginning of each training session ± *SEM*. The timing of fMRI scans performed at 3, 8, and 11 months poststroke relative training are indicated by red dotted lines. Data are shown for both upper left (open circles), upper right (closed circles), and central visual field (green squares) testing. Data are shown for all sessions before the first fMRI scan (during which JS improved rapidly), monthly between Scans 1 and 2 (when performance was relatively constant), and for all sessions between Scans 2 and 3 (when performance gradually approach that of healthy controls). (B) Motion coherence stimulus. A random dot field was placed in a single quadrant of the visual field. For each pair of frames, a proportion of dots (specified by the coherence) were moved translationally (e.g., displaced left/right), whereas the remaining dots were repositioned randomly. (C) Comparison of the size of visual areas V1 and hMT^+ in a control participant C1 and patient JS in fMRI scans collected over multiple sessions (two scans, 6 months apart for C1, scans at 3, 8, and 11 months poststroke for JS). (top) fMRI activation maps in the hMT^+ localization test were projected on axial slices of the structural MRI image, locations of areas V1, hMT^+, and the lesion are shown in the corresponding colors. (bottom) Size of activation (volume) of hMT^+ in response to a central visual field motion coherence stimulus at each fMRI scan.

Measuring Changes in Retinotopic Visual Areas

To assess quantitatively changes in patient JS's retinotopic maps over three fMRI scans obtained at 3, 8, and 11 months after the infarct, during which he underwent training on the motion coherence task, we projected the ROI boundaries and center positions into spherical coordinates. From this, we estimated the geodesic distances on the gray/white matter boundary surface in surface-based coordinate system (Fischl et al., 1999) by computing the arc along the great circle connecting two points (the centers of mass of each ROI assessed in consecutive scans):

$$ds^2 = \left(d\theta^2 + \sin(\theta)d\phi^2\right)r^2$$

where θ is the azimuthal angle in the xy plane from the x axis with $0 \leq \theta \leq 2\pi$, a longitude, and ϕ is the polar angle from the z axis with $0 \leq \phi \leq \pi$, a colatitudes. The

resulting measurement provides the distance along the cortical surface (in mm) between two points, allowing us to assess the distance which an ROI's center of mass shifted between scans. The typical error of estimating distance on the cortex is estimated to be around 10–15% (Fischl et al., 1999).

Voxel-based Correlation of Functional Responses across Scans

To further assess the changes in patterns of organization and response between scans, we computed a voxel-wise correlation analysis within each retinotopic area based on the BOLD response to a full-field checkerboard stimulus. We measured the BOLD percent signal change for each voxel in a given ROI in each of two successive fMRI scans. All voxels in an ROI of the earlier scan were included, even if they were classified within a different retinotopic area in the next scan. We measured the correlation in BOLD response among voxels having positive BOLD signal percent change to determine how stimulus-responsive cortical voxels changed in their responses between scans. Correlation was assessed using a Pearson linear correlation factor, with each data point representing a single voxel.

RESULTS

Behavioral Performance

Motion Coherence Task

Figure 2A shows the thresholds for patient JS during the course of training on this task, obtained from an adaptive staircase (Vaina et al., 2003) at the start of each training sessions. At first patient JS was unable to perceive the stimuli presented to the upper left (affected) quadrant. However, he could achieve a coherence level of roughly 30% if the stimuli were presented to his upper right (unaffected) quadrant, but this level of performance was significantly worse than for the control participants whose thresholds were around 7% ($z = 9.05$, $p < .001$). In the first 5–12 weeks patient JS's performance improved significantly across sessions in both the contralesional ($F = 31.54$, $p = .0025$) and ipsilesional upper visual field quadrants ($F = 27.08$, $p = .002$), reaching 30% and 20%, respectively.

Training continued in the interval between the first and second fMRI scans. Figure 2A shows examples of thresholds obtained on the training days, illustrated in weekly intervals. For stimuli shown in the left upper quadrant contralateral to the lesion there was an initial drop in the threshold indicating some improvement in performance. However performance between 3 and 8 months after the lesion remained relatively flat ($F = 5.8$, $p > .05$). In the third segment of training (8–11 months), there were 17 training sessions, and thresholds for stimuli shown in both upper visual field quadrants were very similar. They show that performance improved significantly in both the left ($F = 30.53$, $p < .001$) and right ($F = 10.95$, $p = .01$) visual fields to below 5% coherence in both quadrants. This level of performance was actually slightly better than that of the healthy controls.

Motion Discontinuity Task

Figure 3 shows the performance of JS on the motion discontinuity task. JS was tested on this task once 1 week before the first fMRI scan, then twice on the same days as two training sessions on motion coherence before the second fMRI scan and again after the second scan. He was initially severely impaired on the task compared with the controls. However, when tested before the second fMRI scan, his thresholds were much lower and similar to the threshold at that time on the motion coherence task. This suggests that the improvement on the motion discontinuity task was because of training on motion coherence such that he was better tuned to the signal provided by the coherent dots.

fMRI during Performance of Motion Tasks

Motion Coherence Task

Figure 2C shows the activations for V1 and hMT$^+$ for patient JS and a control participant. The display, 12° in diameter,

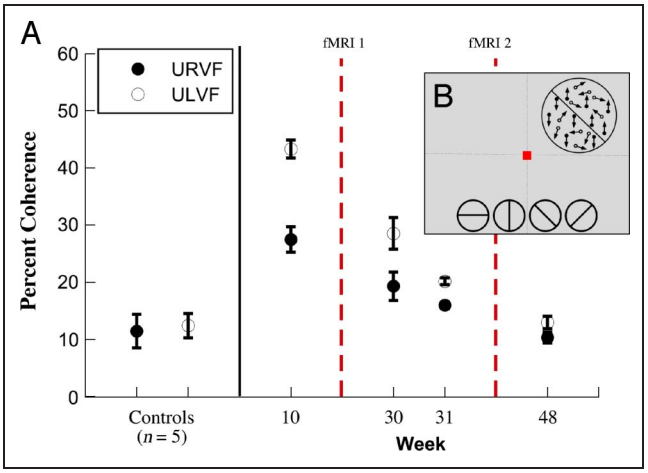

Figure 3. MDT: The motion discontinuity stimulus is shown schematically. The display was either homogeneous (all signal dots moved up or down) or was divided along an illusory horizontal, vertical, or diagonal boundary defined by signal dots on either side of it moving in opposite directions (up or down). In a 2AFC task, participants had to identify whether the motion display was homogeneous (all signal dots moved in the same direction) or whether an illusory boundary traversing the middle of (shown along the bottom 2AFC task). The stimuli, 6° in diameter, were shown in the upper left or right quadrant (B): The figure shows thresholds coherence on the MDT tasks in five healthy participants and in JS. Patient JS took the task four times, a week before the first fMRI scanning at 3 months after the lesion, and then again twice in the week before the second fMRI on this task, and after the second fMRI. The *Y* axis indicates the percent coherence, and the *X* axis, the weeks when patient JS took the psychophysical task.

was presented in the central visual field. Here, the activations shown are for performance of the task with a motion signal (motion coherence) compared with a condition of random motion noise. The motion task (in the ON period) was presented in a constant stimuli paradigm at three coherence levels determined based on the patient's perceptual threshold (shown in green square in Figure 2C).

Activation data are also shown for a representative control participant who was tested twice. In patient JS the number of active voxels in V1 increased over the three testing times. The volume of the activated V1 was 0.05 cm^3 at 3 months after the lesion and 0.31 cm^3 at 11 months after the lesion. There was no significant change in the volume of the activated V1 in the control participant.

In patient JS, the total volume of active voxels in hMT^+ decreased over time in the damaged right hemisphere (from 0.86 cm^3 at 3 months to 0.64 cm^3 at 11 months), and the mean BOLD signal percent change for active voxels ($Z > 3.0$) decreased from 1.51% at 3 months to 0.99% at 11 months. The BOLD value of 0.99% for patient JS in the third scan was similar to the values of 0.91% in the right hemisphere and 0.87% in the left for the control participant. In the normal left hemisphere in patient JS, the volume of BOLD activation decreased more dramatically (from 2.21 cm^3 at 3 months to 1.10 cm^3 at 11 months). There were no significant changes in the control participants in either the left or right hemisphere (Figure 2C shows two consecutive scans in one of the control participants). However, we note that, unlike patient JS, the control participants did not undergo psychophysical training on the motion coherence task between scans, and the percent coherence in the constant stimuli used were identical across the two scans. In JS, the percent coherence changed, according to his threshold obtained before each fMRI scan. At 3 months, patient JS's threshold for central vision was also around 20%, and this was used to guide the choice of constant stimuli during the first fMRI session (15%, 20%, 25% coherence). At 8 months, the staircase threshold for performing the task at 79% correct for stimuli presented in central vision was 13% coherence, and thus, the chosen values for the constant stimuli presented in second fMRI session, at 8 months, were 7%, 13%, 18% coherence, and at 11 months were 4%, 8%, 12%. At this point, patient JS behavioral performance was better than that of the healthy control participants (Figure 2C). The percent coherence used for the healthy control participants was identical to the values used for patients JS at 11 months (4%, 8%, 12%).

Motion Discontinuity Task

Patient JS performed the MDT task at both the 3- and 8-month scans, during which time his psychophysical performance on both the MCT and MDT tests improved dramatically, as shown in Figures 2A and 3A. During fMRI the MDT task (the stimulus was 6° in diameter) was administered in separate runs in the upper right (unaffected) or left (affected) visual field quadrants, in the same locations as they were presented psychophysically. The activations are for performance of the task with a motion signal (MDT test) and the comparison condition of random

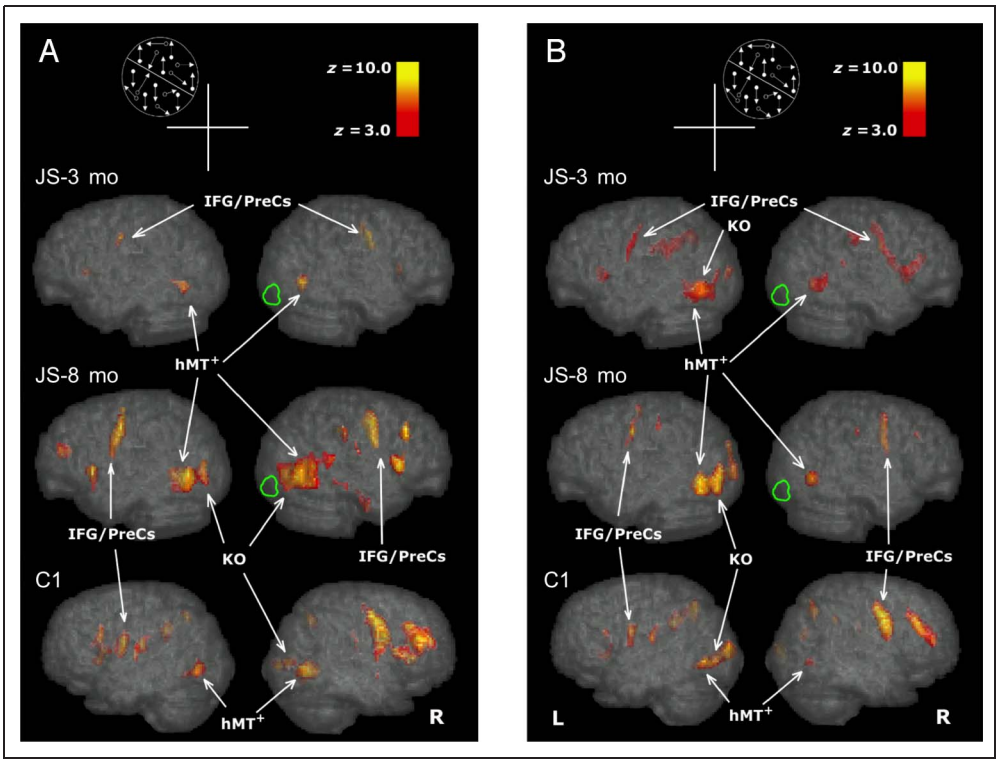

Figure 4. BOLD signal ($Z > 3$) for the MDT displayed on the MNI brain, lateral view of the right and left hemispheres of JS at 3 and 8 months after the lesion and a healthy control (C1-1). The location of the motion discontinuity stimulus, in the upper quandrant ipsilesional or contralesional, is shown schematically in A and B. The arrows point to the activations in the areas hMT^+ and KO. (A) The activations when the stimulus was shown in the upper left visual field quadrant. (B) The activations when the stimulus was shown in the upper left visual field quadrant. IFG = inferior frontal gyrus; preCS = precentral sulcus.

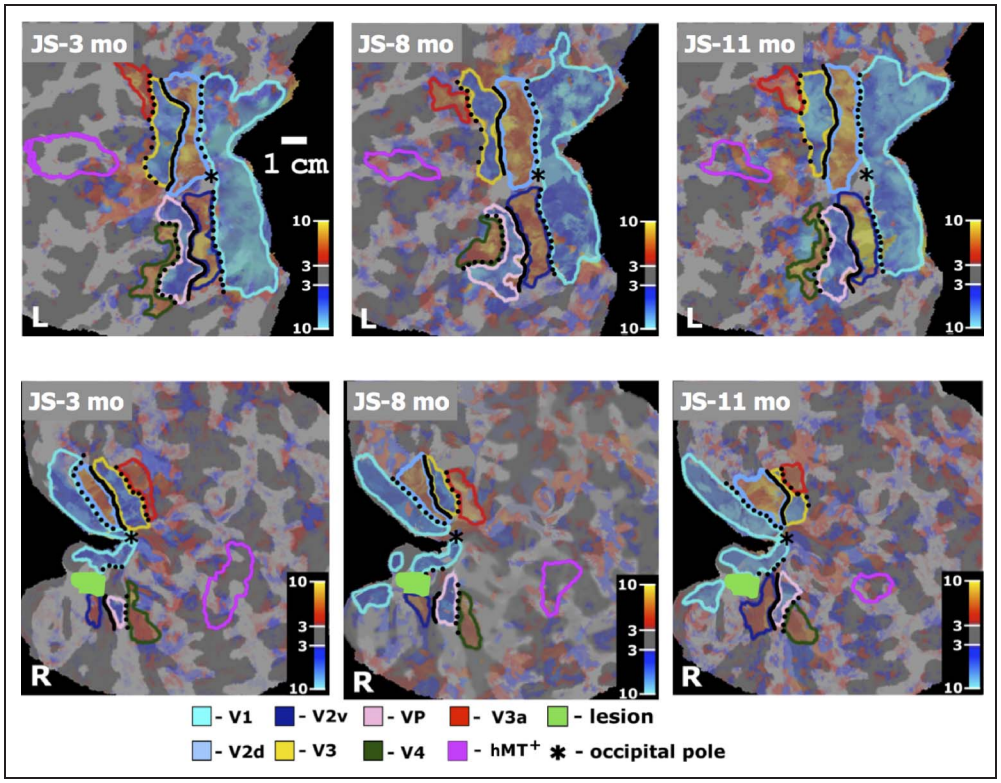

Figure 5. Cortical representation of the tVFS maps of retinotopic visual areas V1, V2d, V2v, V3, VP, V3a, V4, and area hMT$^+$ outlined in different colors (shown in the figure legend) and projected on the flattened representation of the cortical gray matter, separately for the left and right hemisphere. Characteristic alternation pattern of negative and positive field sign areas seen in the representation of the left hemisphere of patient JS. Abnormal retinotopy pattern is seen in the right hemisphere, in which only islands of continuity of the tVFS map representation were found. The intensities of maps are weighted by the *t*-statistical maps identical to the tVFS maps. Cortical representation of the vertical meridian is shown in dotted black line, and representation of the horizontal meridian is shown in solid black line. (JS-3 mo, L) First scan of patient JS, left hemisphere. (JS-8 mo, L) Second scan of patient JS, left hemisphere. (JS-11 mo, L) Third scan of patient JS, left hemisphere. (JS-3 mo, R) First scan of patient JS, right hemisphere. (JS-8 mo, R) Second scan of patient JS, right hemisphere. (JS-11 mo, R) Third scan of patient JS, right hemisphere. The color bar refers to the *t* values of the tVFS maps (significance of the retinotopic response).

motion noise. Guided by perceptual thresholds obtained behaviorally for obtaining 79% correct responses on this task, for patient JS the coherence levels for the constant stimuli in the first scan, were 40% ± 5% for the stimulus shown in the upper left visual field, contralateral to the lesion, and 30% ± 5% for the stimulus shown ipsilateral to the lesion. In the second scan, as patient JS's performance improved, the percent coherence of the constant stimuli in the MDT task were 20% ± 5%. Figure 4 shows the activations in the area hMT$^+$ and also for the earlier visual area KO/V3B in response to the MDT task, known to be involved in computing discontinuity from motion (Van Oostende et al., 1997).

In healthy control participants (Figure 4, bottom row, representative control participant), we found that the MDT task primarily activated the contralateral hMT$^+$ and KO and also slightly activated the ipsilateral hMT$^+$. When the stimulus was presented to the upper left visual

Table 1. Relative ROI Size between Hemispheres (Ratio of Ipsilesional to Contralesional Surface Area) for Patients JS and PF and a Healthy Control (C1)

ROI	*JS I/C 0–3 months*	*JS I/C 3–8 months*	*JS I/C 8–11 months*	*PF I/C 0–3 months*	*PF I/C 0–7 months*	*C1 RH/LH 0 month*	*C1 RH/LH 0–6 months*
V1	**0.37**	**0.48**	**0.52**	**0.88**	**1.71**	0.78	0.83
V2v	**0.19**	**0.17**	**0.52**	**0.08**	**0.08**	0.95	0.92
V2d	0.58	0.59	0.74	0.62	1.66	1.28	1.29
V3v/VP	**0.21**	**0.40**	**0.48**	1.31	0.84	0.92	0.96
V3	0.94	0.61	0.38	1.12	0.74	1.38	1.30
V3a	1.57	1.50	0.79	0.92	0.98	0.98	1.12
V4	0.85	0.75	0.66	1.45	1.30	1.16	1.21
hMT$^+$	0.90	0.89	0.64	0.90	0.96	0.64	0.66

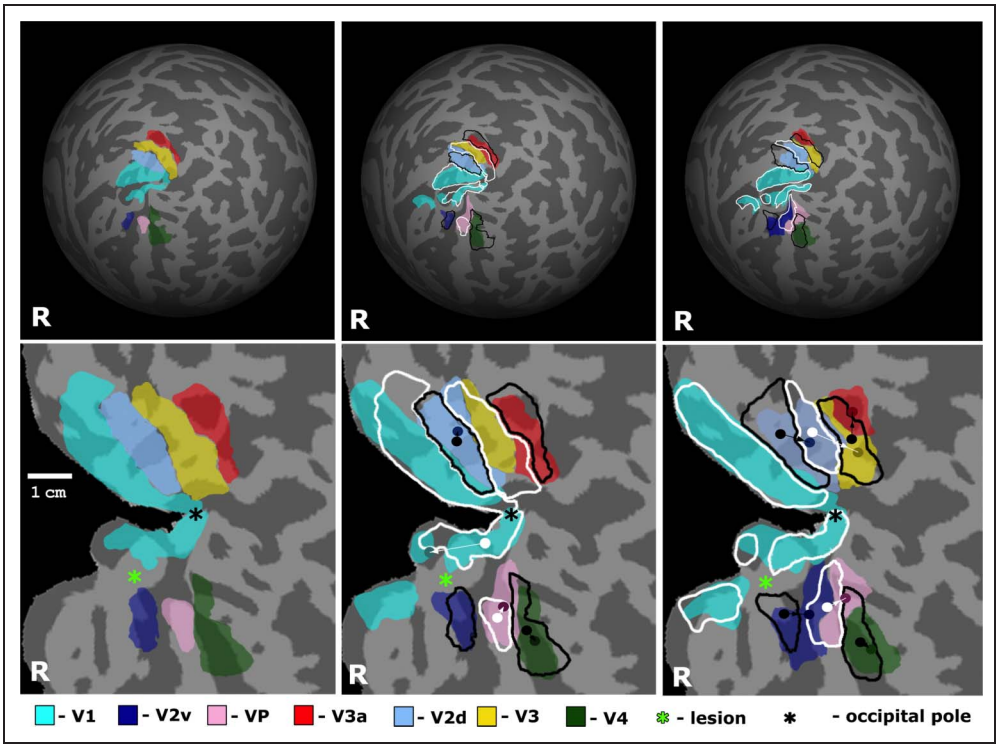

Figure 6. Reorganization of retinotopic visual areas in the affected (right) hemisphere of patient JS shown on the reconstructed brain surface. Areas V1, V2d, V2v, V3, VP, V3a, and V4 are shown in different semitransparent colors as specified in the figure legend. Location and size of visual areas in the previous scan is outlined in white or black for negative field sign and positive field sign areas, respectively. (top) Overtime changes in retinotopic visual areas registered in spherical coordinate system. Data from three scans of patient JS are shown: JS-3, 8 and 11 months. (bottom) Overtime changes in retinotopic visual areas overlaid on the flattened representation of the occipital cortex. Locations of the center of mass of areas V2d, V2v, V3, VP, V3a, and V4 are shown by dots having same color as specified in the figure legend but decreased brightness. Locations of the center of mass of the same areas in the previous scan are shown by white or black dots for negative field sign and positive field sign areas correspondingly. Directions of reorganization of retinotopic areas V2d, V2v, V3, VP, V3a, and V4 are shown by arrows. The table shows the distance of shifts of the center of mass (in mm) estimated in spherical coordinates for the above retinotopic areas in the lesioned right hemisphere, between the first and second scan (top row) and between the second and third scan (bottom row). The shifts in JS's normal left hemisphere and in healthy controls are shown in Table 2.

field, the volume of activated hMT^+ was 5.57 cm^3 in the right hemisphere and 5.51 cm^3 in the left hemisphere. When the stimulus was presented to the upper right visual field, the volume of activated hMT^+ was 6.50 cm^3 in the left hemisphere and 3.22 cm^3 in the right.

Activation in KO was seen contralaterally (4.86 and 3.63 cm^3 for the upper left and right fields, respectively), but there was no ipsilateral activation in response to either visual field condition.

Figure 4A (top two rows) shows the activation for the motion discontinuity stimulus presented in the upper left (affected) quadrant in patient JS at 3 and 8 months after the right hemisphere infarct. At 3 months, the volume of activated hMT^+ was 6.80 cm^3 in the right hemisphere and 5.86 cm^3 in the left hemisphere. There was no significant activation in area KO in either hemisphere. At 8 months, the volume of activation had increased to 10.49 cm^3 in the lesioned right hemisphere and to 6.15 cm^3 in the left hemisphere. Area KO was now significantly activated in both hemispheres, with a volume of 5.92 cm^3 in the right hemisphere and 4.92 cm^3 in the left.

Table 2. Shift in ROI Center of Mass (mm) between Successive Scans for Patient JS and a Healthy Control (C1)

ROI	*JS I (RH) 3–8 months*	*JS I (RH) 8–11 months*	*JS C (LH) 3–8 months*	*JS C (LH) 8–11 months*	*C1 RH 0–6 months*	*C1 LH 0–6 months*
V2v	**0.8**	**1.7**	1.5	1.5	0.0	0.2
V2d	1.5	5.2	0.8	0.8	0.0	0.5
V3v/VP	**3.8**	**4.9**	1.5	1.2	0.5	0.5
V3	0.6	6.9	0.4	0.0	0.2	0.0
V3a	1.6	4.1	1.1	1.5	0.2	0.2
V4	1.5	3.7	1.9	1.2	0.5	0.2

Figure 4B (top two rows) shows the activation for the motion discontinuity stimulus presented in the upper right (nonaffected) quadrant in patient JS at 3 and 8 months after the right hemisphere infarct. At 3 months, the volume of activated hMT^+ was 14.65 cm^3 in the left hemisphere and 4.75 cm^3 in the right hemisphere. Area KO was significantly activated in the left hemisphere, with a volume of 4.10 cm^3. At 8 months, the volume of activated hMT^+ was 10.84 cm^3 in the left hemisphere and 5.04 cm^3 in the right hemisphere. Area KO was significantly activated in the left hemisphere, with a volume of 4.63 cm^3. The critical finding relates to the difference in the activation in hMT+ and KO in the affected (right) hemisphere compared with the unaffected (left) hemisphere when the display was presented contralaterally in each case. At 3 months the difference was -7.85 cm^3 for hMT+ and -4.10 cm^3 for KO, whereas at 8 months it was -0.35 cm^3 for hMT+ and 1.29 cm^3 for KO. In other words the activation in the affected hemisphere was subnormal at 3 months but normalized by 8 months.

Retinotopic Mapping

Patient JS

Figure 5 shows the retinotopic areas for patient JS in the scans at 3, 8, and 11 months after his infarct. For each scan, we measured the size and center of mass of each retinotopic area. To arrive at a quantitative assessment of the change in the surface of the areas, we used the intact hemisphere as a reference and measured the extent in the ipsilesional and contralesional hemisphere. Table 1 presents the data for the ipsilesional/contralesional (I/C) ratio for each area. We used the center of mass of each area to determine whether there was a shift across scans over time.

In the initial scan, there was a significant reduction in the activated area of V1, V2v, and VP in the lesioned compared with JS's normal hemisphere, with I/C ratios of 0.37, 0.19, and 0.21, respectively. There was also a minor reduction in V2d with an I/C ratio of 0.58. The reduction was expected for areas V1, V2v, and VP because they were involved in the lesion. The reduction in the V2d could either be because of damage that is not evident or to a loss of input from earlier areas.

Over the course of the following months, there was substantial recovery of surface area in all these areas (Table 1). The I/C ratio for V1 increased from 0.37 to 0.48 to 0.52 over the three scans. The corresponding ratios for area V2v were 0.19, 0.17, and 0.52, and for area V2d 0.58, 0.59, and 0.74. Area VP or V3v also increased progressively over the three scans, from 0.21 to 0.40 to 0.48.

The pattern was different for the retinotopic areas that are higher in the hierarchy of visual processing. Initially, areas V4 in the ventral stream and V3 in the dorsal stream were as extensive in the right as the left hemisphere, and V3a in the dorsal stream was more extensive in the right hemisphere. In the first scan, the I/C ratios in these areas were 0.85, 0.94, and 1.57, respectively. However, by the third scan, the I/C ratios were reduced to 0.66, 0.38, and 0.79, respectively.

Given all these changes, we were interested in whether there were also shifts in the center of mass of each ROI. We measured the shift along the cortical surface using a spherical coordinate projection. This is as shown in Figure 6A and as described in the Methods.

Figure 6 illustrates the magnitude of shifts of the center of mass in each retinotopic areas in the lesioned (right) hemisphere. In several ROIs, the shift of the center of mass was consistent with the changes in surface area as reported in Table 1. These shifts were most marked between 8 and 11 months. In the time between the first and second scans, only area VP showed a significantly larger shift, of 3.8 mm, than in the intact hemisphere and in the normal controls (Table 2). However, in the interval between the second and third scans, there were shifts ranging from 1.7 mm in V2v to 6.9 mm in V3 (Figure 6, Table 2). By contrast in the intact left hemisphere of patient JS, the shifts were small with a maximum of 1.5 mm and they did not show any systematic pattern. Furthermore, in the control participant, the shifts were negligible, of the order of less than 0.5 mm (Table 2).

This trend is also seen in the retinotopic occipital areas in the analysis of the correlations between the BOLD responses of voxels across scans in the full field checkerboard stimulus (Table 3). We used voxel-wise correlation in the BOLD response to a full-field checkerboard stimulus to examine the consistency of responses of voxels in retinotopic areas V2v, V2d, and V3/VP (Figure 7 and Table 3). In the lesioned right hemisphere he variability in response between the 3- and 8-month scans was much higher compared with the control participant in both V2d ($r_R = 0.4$) and V2v ($r_R = 0.2$), but it was largely reduced between the 8- and 11-month scans ($r_R = 0.7$, 0.4 for

Table 3. Normalized Cross-correlation Coefficients Calculated between BOLD Signal Percent Change in the Full-field Checkerboard Stimulus (for V2v, V2d, VP, and V3) and the MT Localizer (for hMT^+) Used in the Scatter Plots above

	V2v (l/r)	*V2d (l/r)*	*VP (l/r)*	*V3 (l/r)*	*hMT+ (l/r)*
C1-1 vs. C1-2	1.0/1.0	1.0/0.9	1.0/1.0	1.0/1.0	0.9/0.7
JS-3 months vs. JS-8 months	0.9/0.4	0.8/0.2	0.9/0.7	0.9/0.8	0.3/0.6
JS-8 months vs. JS-11 months	0.9/0.7	0.9/0.4	1.0/0.7	0.8/0.5	0.5/0.8

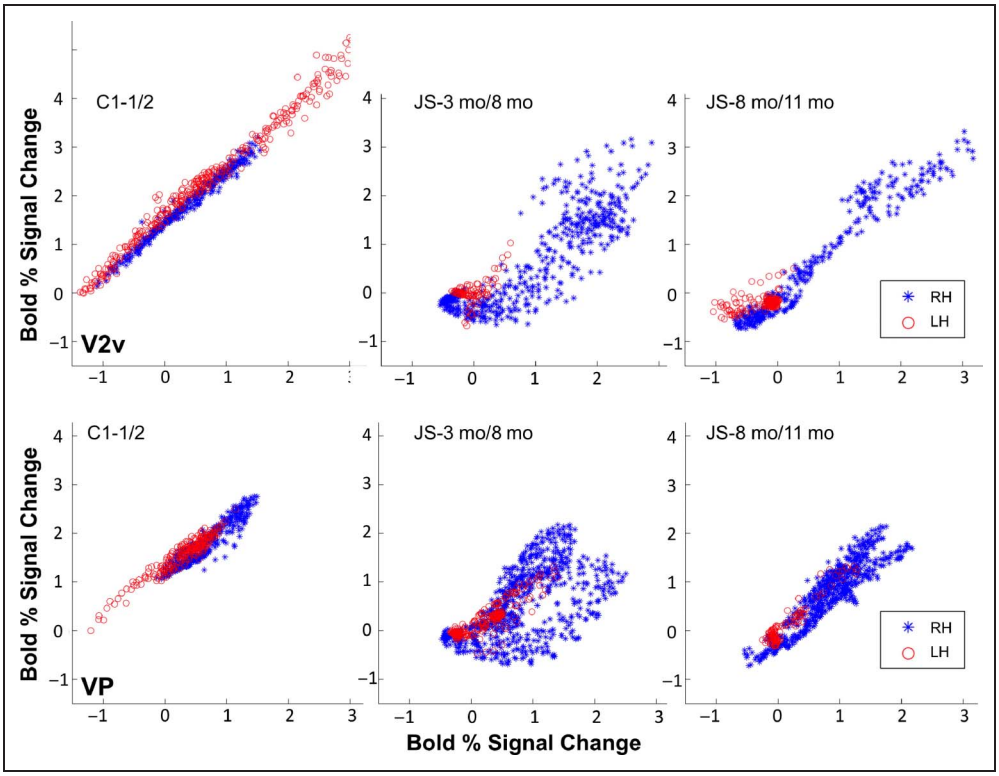

Figure 7. Scatter plots for areas (top) V2v and (bottom) VP as defined by retinotopy mapping. *X*- and *Y*-axis values indicate % BOLD signal change for voxels in the ROI at the earlier time point for the two consecutive scans. Left hemisphere scatter plot is shown in red asterisks; right hemisphere scatter plot is shown in blue circles. Coefficients of correlation for ROI defined for both hemispheres are printed on each plot. Correlation values for areas V2v, V2d, VP, and V3 in both hemispheres are given in Table 3.

V2d and V2v), and almost no variability was observed in the intact, left hemisphere ($r_L \geq 0.8$ for V2d and V2v in both intervals). These results suggest that the weak correlations were specific to the damaged hemisphere and were observed mainly within the scans performed within the first 8 months following stroke.

In areas V3 and VP, we again found weakened correlations in JS's lesioned right hemisphere (but not in the normal left hemisphere) compared with the control (Table 3), but unlike V2d/v, the correlations did not improve between the later scans. The consistency in activation in area V3 decreased ($r_R = 0.8–0.5$) over the later time period (8–11 months). Thus, whereas V2d/v showed a return to higher activation consistency after 8 months, V3 and VP continued to show a high degree of variability.

Patient PF

In this patient, the lesion was in the left hemisphere. In this patient, therefore, the I/C ratio compares the areas in the left (ipsilesional) with the right (contralesional) hemisphere. As in patient JS, the lesion extended from V1 to V2v, but as can be seen from Figure 4, area V2v was almost completely eradicated in the left hemisphere.

Figure 8 shows the results for retinotopic mapping, and Table 1 gives the I/C ratios for the two scans. Initially, the area of activated V1 was slightly reduced in size with an I/C of 0.88, but there was almost no evidence of an activated V2v in the affected hemisphere with an I/C ratio of 0.08). However, by the second scan, the ratio for V1

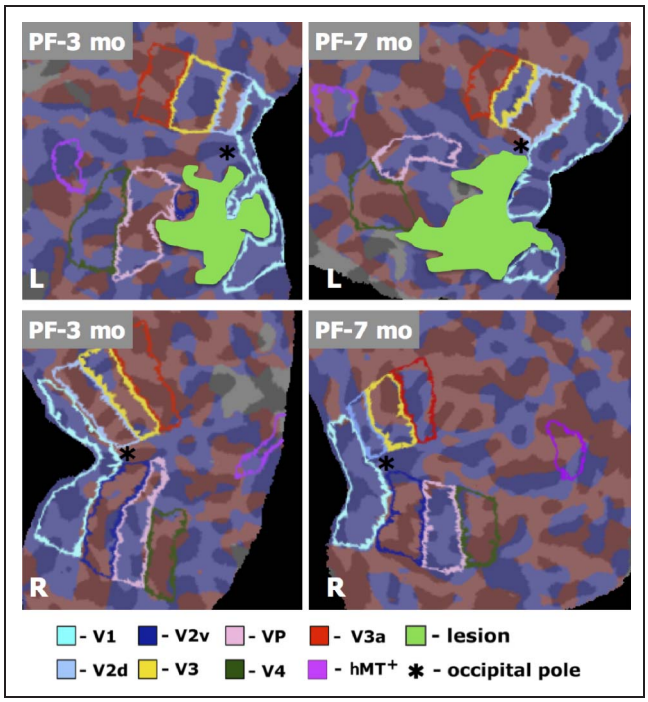

Figure 8. Retinotopic maps for a retrospective patient study (patient PF), computed based on the standard FreeSurfer pipeline (Engel et al., 1994, 1997; DeYoe et al., 1996; Sereno et al., 1995), using the same stimulus as presented to patient PF and the control. Data were acquired 3 and 7 months poststroke, and visual areas were identified by mapping the polar and eccentricity maps to the cortical surface and identifying field sign boundaries. Borders were identified automatically in FreeSurfer and confirmed by manual inspection. Visual areas are shown in different colors (see legend), with the lesion shown in solid green.

was 1.71; in other words, the activated V1 was now larger in the affected hemisphere. The results for V2v remained unchanged.

By the second scan, there was a significant increase in the I/C ratio of V2d; the ratio was 0.62 at Scan 1 and 1.66 at Scan 2. As in patient JS, there were decreases in some areas later in the hierarchy of visual processing. The ratios for VP or V3v went from 1.31 to 0.84 and for V3 from 1.12 to 0.98.

DISCUSSION

The Introduction asked three questions. The first was whether the sort of changes reported in animals after lesions can be found in patients. It is clear that they can. Eysel (2009) found that after a striate lesion in cats there is an increase in the receptive fields of neurons adjacent to the lesion. Zepeda et al. (Zepeda, Sengpiel, Guagnelli, Vaca, & Arias, 2004; Zepeda, Vaca, Arias, & Sengpiel, 2003) used both cell recording and optical imaging to show that after a striate lesion in kittens there is an expansion in the representation of visual space in the surrounding area.

We studied patient JS who has a lesion in V1, extending into V2v and VP. This lesion caused an upper left quadrantanopia (Figure 1C) consistent with his ventral, occipital lobe lesion. As in the experiments by Zapeda et al. on cats, there was a decrease at first in the extent of V1 in the lesioned hemisphere, but with time this area increased markedly. The increase continued over a period of 11 months after the infarct.

The spatial resolution of fMRI is not good enough to make a definitive judgment about where within V1 the changes occurred. However, fMRI has the advantage over single unit recording that it is a whole-brain method. This means that we have been able to show that similar changes occurred in the other areas on which the lesion encroached. In the case of JS, these were V2v and VP. There was also an increase in these areas over time.

These increases appear to have been at the expense of adjacent areas. We noted significant decreases in V3 and V3a. Baseler, Morland, and Wandell (1999) have suggested that, when neurons in an area lose their normal inputs, they can be "colonized" by other neurons in neighboring cortex, meaning that they can become responsive to new inputs. Baseler et al. further suggest that this effect is mediated by horizontal connections. They carried out retinotopic mapping in a patient with a large lesion of V1 that extended into V2v and VP and report reorganization of the retinotopy in V2d and V3d. Although colonization of this sort might occur between neurons within an area, further research is needed to see if it can occur for neurons in different areas.

To document the retinotopic changes, we have compared the size of the different areas in the lesioned and nonlesioned hemisphere (Table 1). This has the advantage that the nonlesioned hemisphere acts as a control, thus providing a measure of the test–retest reliability of the mapping. Although such a test is also provided by retinotopic mapping in healthy participants, the use of the nonlesioned hemisphere in patients serves as a more rigorous test because it is carried out in an abnormal brain.

As well as changes in size, we observed shifts in retinotopic area location (Figure 6). There were shifts in the center of mass of the order of 5 mm or more (Table 2). The data showed significant reductions in the response correlation in the damaged hemisphere's V2d/v between the 3- and 8-month scans and in V3 and VP in the damaged hemisphere, persisting beyond 8 months postinfarct. The time frame for reorganization in the areas V2d/v was restricted to the time interval between the first two scans (3 and 8 months), as shown by the substantially reduced correlations between these time points. Negligible changes were seen between 8 and 11 months. On the other hand, the correlations in V3 and VP remained low throughout, suggesting continued reorganization after the 8-month mark. Further data are needed to more fully assess these points, but they are suggestive of lesion-driven plasticity in visual cortex in conjunction with the changes in ROI area and location and point to specific time frames over which such changes occur.

The second question posed in the Introduction was what effect any changes in early visual areas have on the activity of higher areas involved in detecting the direction in motion coherence displays. Collins et al. (2003) recorded in MT in monkeys with subtotal striate lesions and found that neurons in the deprived zone did not respond to coherent motion. However, they suggest that some partially deprived neurons may have acquired new receptive fields. Rosa, Tweedale, and Elston (2000) also reported that there were neurons in the deprived zone that had displaced receptive fields. Functional imaging does not have the spatial resolution to detect the border of the deprived zone. However, as already mentioned, it has the advantage of being a whole-brain method.

In patient JS, the MCT task was used to localize hMT^+. In fMRI, the MCT displays, 12° in diameter, were presented in central vision. The activations are the results of a comparison between performing the task with a directional motion signal and a comparison condition with a nondirectional motion noise. The activation volume in hMT^+ was initially higher than in controls, but it reduced to the levels of the normal controls in the second and third scans (Figure 2C). In between scans patient JS underwent training on the motion coherence task, with stimuli presented to the upper left and right quadrants (Figure 2A). There are two possible explanations of this decrease. The problem is that there are two factors that could influence the degree of activation. The first is the degree of motion coherence in the displays. Because patient JS improved on the task from 3 to 8 to 11 months, the degree of coherence in the displays presented during those scanning sessions also decreased (consistent with the threshold of percent coherence to perform the task in the condition

used in fMRI) because the task was always given at threshold, and the patient's thresholds improved. Rees, Friston, and Koch (2000) report that the activation in hMT^+ decreased linearly as motion coherence decreased. However, there is a second potential factor. This is that JS received extensive training on the task, and the decrease could reflect some aspect of perceptual learning. It is not clear whether perceptual learning with RDKs involves learning to respond to the relevant feature of the displays or learning to ignore the irrelevant feature, that is, the noise (Vaina, Sundareswaran, & Harris, 1995). It is not possible to evaluate the ways in which learning and the change in the coherence these two factors might interact in our data.

The critical observation concerning the fate of higher areas after a lesion early in the system relates to the MDT task on which patient JS was not trained. Here the displays (6° in diameter) were presented either to the affected or to the unaffected upper quadrants. The activations are the results of a comparison between performing the task with a directional motion signal and a comparison condition with motion noise (nondirectional). In patient JS, the activation in both hMT^+ and KO increased in the lesioned hemisphere (Figure 4) in the second scan, 8 months after the lesion. This is at odds with what would have been expected from the fact that the percent coherence of the stimulus decreased between the two scans. Thus, the increases we observed in both hMT^+ and KO appear to genuinely relate to the improvement in behavioral performance.

The normalization of the activation in hMT+ and KO occurred in parallel with the changes in early visual areas in the affected hemisphere. There were two changes in earlier retinotopic areas in patient JS. The first was the increase in the area of responsivity in the lesioned region, including V1, to the rotating wedge and expanding rings stimuli. The second was the very significant increase in the area of responsiveness in V1 over the three scans when the patient was presented with the motion coherence displays. It would be important to know whether one can relate the changes in hMT^+ and KO and the associated behavioral recovery to the retinotopic changes. However, to find out one would need to see if there are cases of recovery but no changes in retinotopy or if there are cases of changes in retinotopy but no recovery. Further research is therefore needed to discover if it possible to establish cause and effect.

The final question was whether training promotes recovery. As explained in the Introduction, we tried to tackle this question by finding a patient with a similar lesion who had not been formally trained on the motion tasks. Unfortunately, because patient PF was chosen retrospectively, the methods for analyzing the retinotopic mapping were not identical to those used with patient JS. As explained in the Methods section, the technique devised by Dumoulin et al. (2003) was used with JS but not with PF. Nonetheless, we take it as significant that in patient PF there were marked changes in retinotopy over time. However, this patient was only tested at 3 and 7 months after the infarct, whereas the largest shifts in patient JS occurred between 8 and 11 months after the infarct. It could be that these simply correspond to the third stage of recovery described by Churchill et al. (1998), but we cannot discount the possibility that they were promoted by formal training on the motion coherence task.

That training might have such an effect is suggested by the nature of the mechanisms that underlie the changes in responsivity over time. After a stroke, there are physiological changes such that neurons become more excitable and susceptible to LTP (Carmichael, 2003). Furthermore, there is speculation that there are common mechanisms for the cortical changes that occur with injury, activity, and experience (Overman & Carmichael, 2013). There are even suggestions that changes in cortex may recapitulate ones that occur early in development (Mowery & Garraghty, 2009). If so, training might indeed promote the rebuilding of circuits.

That it might do so is not the same as saying that we know that it does so. Nor do we pretend to have carried out a proper test of the effects of training. In everyday life, patient PF would have been exposed to visual experiences that might promote cortical changes. However, we distinguish such experience from the potential effects of formal training such as that received by patient JS. It would clearly be worth carrying out a proper trial in which retinotopic mapping is performed repeatedly as in the present article, but with two groups of patients of which one is trained and the other is not.

Acknowledgments

This work was supported by NIH grant R01NS064100 to L. M. V. Lucia M. Vaina dedicates this article to Charlie Gross, who has been a long-time collaborator and friend. I met him at the INS meeting in Beaune (France), and since then we often discussed the relationship between several aspects of high-level visual processing described in his work in monkeys physiology and my work in neuropsychology. In particular, his pioneering study of biological motion in monkeys' superior temporal lobe has influenced my own work on biological motion and has led us to coauthor a paper on this topic. Working with Charlie was a uniquely enjoyable experience. Alan Cowey and I often spoke fondly about Charlie, a dear friend and close colleague to us both, whose work, exquisite sense of humor, and unbound zest of living we both deeply admired and loved.

Reprint requests should be sent to Lucia M. Vaina, Departments of Biomedical and Neuroscience, Boston University, Room 315, 44 Cummington Street, Boston, MA 02215, or via e-mail: vaina@bu.edu.

REFERENCES

Azzopardi, P., & Cowey, A. (2001). Motion discrimination in cortically blind patients. *Brain; A Journal of Neurology, 124,* 30–46.

Baseler, H. A., Morland, A. B., & Wandell, B. A. (1999). Topographic organization of human visual areas in the absence of input from primary cortex. *Journal of Neuroscience, 19,* 2619–2627.

Braddick, O. J., O'Brien, J. M., Wattam-Bell, J., Atkinson, J., Hartley, T., & Turner, R. (2001). Brain areas sensitive to coherent visual motion. *Perception, 30,* 61–72.

Calford, M. B., Chino, Y. M., Das, A., Eysel, U. T., Gilbert, C. D., Heinen, S. J., et al. (2005). Neuroscience: Rewiring the adult brain. *Nature, 438,* E3; discussion E3-4.

Carmichael, S. T. (2003). Plasticity of cortical projections after stroke. *Neuroscientist, 9,* 64–75.

Chen, L. M., Qi, H. X., & Kaas, J. H. (2012). Dynamic reorganization of digit representations in somatosensory cortex of nonhuman primates after spinal cord injury. *Journal of Neuroscience, 32,* 14649–14663.

Chino, Y. M. (1995). Adult plasticity in the visual system. *Canadian Journal of Physiology and Pharmacology, 73,* 1323–1338.

Churchill, J. D., Muja, N., Myers, W. A., Besheer, J., & Garraghty, P. E. (1998). Somatotopic consolidation: A third phase of reorganization after peripheral nerve injury in adult squirrel monkeys. *Experimental Brain Research, 118,* 189–196.

Churchill, J. D., Tharp, J. A., Wellman, C. L., Sengelaub, D. R., & Garraghty, P. E. (2004). Morphological correlates of injury-induced reorganization in primate somatosensory cortex. *BMC Neuroscience, 5,* 43.

Collins, C. E., Lyon, D. C., & Kaas, J. H. (2003). Responses of neurons in the middle temporal visual area after long-standing lesions of the primary visual cortex in adult new world monkeys. *Journal of Neuroscience, 23,* 2251–2264.

Dale, A. M., Fischl, B., & Sereno, M. I. (1999). Cortical surface-based analysis. I. Segmentation and surface reconstruction. *Neuroimage, 9,* 179–194.

DeYoe, E. A., Carman, G. J., Bandettini, P., Glickman, S., Wieser, J., Cox, R., et al. (1996). Mapping striate and extrastriate visual areas in human cerebral cortex. *Proceedings of the National Academy of Sciences, U.S.A., 93,* 2382–2386.

Dumoulin, S., Bitta, R., Kabani, N., Baker, C., Goualher, G., Pike, G., et al. (2000). A new anatomical landmark for reliable identification of human area V5/Mt: A quantitative analysis of sulcal patterning. *Cerebral Cortex, 10,* 454–463.

Dumoulin, S. O., Hoge, R. D., Baker, C. L., Hess, R. F., Achtman, R. L., & Evans, A. C. (2003). Automatic volumetric segmentation of human visual retinotopic cortex. *Neuroimage, 18,* 576–587.

Dupont, P., De Bruyn, B., Vandenberghe, R., Rosier, A., Michiels, J., Marchal, G., et al. (1997). The kinetic occipital region in human visual cortex. *Cerebral Cortex, 7,* 283–292.

Engel, S. A., Glover, G. H., & Wandell, B. A. (1997). Retinotopic organization in human visual cortex and the spatial precision of functional MRI. *Cerebral Cortex, 7,* 181–192.

Engel, S. A., Rumelhart, D. E., Wandell, B. A., Lee, A. T., Glover, G. H., Chichilnisky, E. J., et al. (1994). fMRI of human visual cortex. *Nature, 369,* 525.

Eysel, U. T. (2009). Adult cortical plasticity. In *Encyclopedia of neusroscience* (pp. 141–147). New York: Academic Press.

Fischl, B., Liu, A., & Dale, A. M. (2001). Automated manifold surgery: Constructing geometrically accurate and topologically correct models of the human cerebral cortex. *IEEE Transactions on Medical Imaging, 20,* 70–80.

Fischl, B., Sereno, M. I., & Dale, A. M. (1999). Cortical surface-based analysis. II: Inflation, flattening, and a surface-based coordinate system. *Neuroimage, 9,* 195–207.

Fischl, B., van der Kouwe, A., Destrieux, C., Halgren, E., Segonne, F., Salat, D. H., et al. (2004). Automatically parcellating the human cerebral cortex. *Cerebral Cortex, 14,* 11–22.

Friston, K. J., Jezzard, P., & Turner, R. (1994). Analysis of functional MRI time series. *Human Brain Mapping, 1,* 153–171.

Garraghty, P. E., Arnold, L. L., Wellman, C. L., & Mowery, T. M. (2006). Receptor autoradiographic correlates of deafferentation-induced reorganization in adult primate somatosensory cortex. *Journal of Comparative Neurology, 497,* 636–645.

Garraghty, P. E., & Kaas, J. H. (1991). Large-scale functional reorganization in adult monkey cortex after peripheral nerve injury. *Proceedings of the National Academy of Sciences, 88,* 6976–6980.

Greenlee, M. W. (2000). Human cortical areas underlying the perception of optic flow: Brain imaging studies. *International Review of Neurobiology, 44,* 269–292.

Huxlin, K. R., Martin, T., Kelly, K., Riley, M., Friedman, D. I., Burgin, W. S., et al. (2009). Perceptual relearning of complex visual motion after V1 damage in humans. *Journal of Neuroscience, 29,* 3981–3991.

Jain, N., Qi, H. X., Collins, C. E., & Kaas, J. H. (2008). Large-scale reorganization in the somatosensory cortex and thalamus after sensory loss in macaque monkeys. *Journal of Neuroscience, 28,* 11042–11060.

Merzenich, M. M., Nelson, R. J., Stryker, M. P., Cynader, M. S., Schoppmann, A., & Zook, J. M. (1984). Somatosensory cortical map changes following digit amputation in adult monkeys. *Journal of Comparative Neurology, 224,* 591–605.

Moore, T., Rodman, H. R., & Gross, C. G. (2001). Direction of motion discrimination after early lesions of striate cortex (V1) of the macaque monkey. *Proceedings of the National Academy of Sciences, U.S.A., 98,* 325–330.

Morrone, M. C., Tosetti, M., Montanaro, D., Fiorentini, A., Cioni, G., & Burr, D. C. (2000). A cortical area that responds specifically to optic flow, revealed by fMRI. *Nature Neuroscience, 3,* 1322–1328.

Mowery, T. M., & Garraghty, P. E. (2009). Nerve-injury induced changes to GluR1 and GluR2/3 sub-unit expression in area 3b of adult squirrel monkeys: Developmental recapitulation? *Frontiers in Systems Neuroscience, 3,* 1.

Newsome, W. T., & Paré, E. B. (1988). A selective impairment of motion perception following lesions of the middle temporal visual area (MT). *Journal of Neuroscience, 8,* 2201–2211.

Overman, J. J., & Carmichael, S. T. (2013). Plasticity in the injured brain: More than molecules matter. *Neuroscientist*.

Pelli, D. G. (1997). The VideoToolbox software for visual psychophysics: Transforming numbers into movies. *Spatial Vision, 10,* 437–442.

Rees, G., Friston, K., & Koch, C. (2000). A direct quantitative relationship between the functional properties of human and macaque V5. *Nature Neuroscience, 3,* 716–723.

Reese, T. G., Davis, T. L., & Weisskoff, R. M. (1995). Automated shimming at 1.5 Tesla using echo planar image frequency maps. *Journal of Magnetic Resonance Imaging, 5,* 739–745.

Rodman, H. R., Gross, C. G., & Albright, T. D. (1989). Afferent basis of visual response properties in area MT of the macaque. I. Effects of striate cortex removal. *Journal of Neuroscience, 9,* 2033–2050.

Rosa, M. G., Tweedale, R., & Elston, G. N. (2000). Visual responses of neurons in the middle temporal area of new world monkeys after lesions of striate cortex. *Journal of Neuroscience, 20,* 5552–5563.

Rutschmann, R., Schrauf, M., & Greenlee, M. W. (2000). Brain activation during dichoptic presentation of optic flow stimuli. *Experimental Brain Research, 134,* 533–537.

Sereno, M. I., Dale, A. M., Reppas, J. B., Kwong, K. K., Belliveau, J. W., Brady, T. J., et al. (1995). Borders of multiple visual areas in humans revealed by functional magnetic resonance imaging. *Science, 268,* 889–893.

Slotnick, S. D., Moo, L. R., Krauss, G., & Hart, J., Jr. (2002). Large-scale cortical displacement of a human retinotopic map. *NeuroReport, 13,* 41–46.
Smirnakis, S. M., Brewer, A. A., Schmid, M. C., Tolias, A. S., Schuz, A., Augath, M., et al. (2005). Lack of long-term cortical reorganization after macaque retinal lesions. *Nature, 435,* 300–307.
Tootell, R. B., Mendola, J. D., Hadjikhani, N. K., Liu, A. K., & Dale, A. M. (1998). The representation of the ipsilateral visual field in human cerebral cortex. *Proceedings of the National Academy of Sciences, U.S.A., 95,* 818–824.
Vaina, L. M., Cowey, A., Eskew, R. T., LeMay, M., & Kemper, T. (2001). Regional cerebral correlates of global motion perception: Evidence from unilateral cerebral brain damage. *Brain, 124,* 310–321.
Vaina, L. M., Gryzwacz, N. M., Saiviroonporn, P., LeMay, M., Bienfang, D. C., & Cowey, A. (2003). Can spatial and temporal motion integration compensate for deficits in local motion mechanisms? *Neuropsychologia, 41,* 1817–1836.
Vaina, L. M., LeMay, M., Bienfang, D. C., Choi, A. Y., & Nakayama, K. (1990). Intact "biological motion" and "structure from motion" perception in a patient with impaired motion mechanisms: A case study. *Visual Neuroscience, 5,* 353–369.
Vaina, L. M., Sikoglu, E. M., Soloviev, S., Lemay, M., Squatrito, S., Pandiani, G., et al. (2010). Functional and anatomical profile of visual motion impairments in stroke patients correlate with fMRI in normal subjects. *Journal of Neuropsychology, 4,* 121–145.
Vaina, L. M., & Soloviev, S. (2004). Functional neuroanatomy of self-motion perception in humans. In L. M. Vaina, S. A. Beardsley, & S. Rushton (Eds.), *Optic flow and beyond* (pp. 109–137). Dordrecht: Kluwer Academic Press.
Vaina, L. M., Sundareswaran, V., & Harris, J. G. (1997). Learning to ignore: Psychophysics and computational modeling of fast learning of direction in noisy motion stimuli. *Cognitive Brain Research, 2,* 155–163.
Van Oostende, S., Sunaert, S., Van Hecke, P., Marchal, G., & Orban, G. A. (1997). The kinetic occipital (KO) region in man: An fMRI study. *Cerebral Cortex, 7,* 690–701.
Wandell, B. A. (1999). Computational neuroimaging of human visual cortex. *Annual Review of Neuroscience, 22,* 145–173.
Wandell, B. A., Dumoulin, S. O., & Brewer, A. A. (2007). Visual field maps in human cortex. *Neuron, 56,* 366–383.
Woods, R. P., Cherry, S. R., & Mazziotta, J. C. (1992). Rapid automated algorithm for aligning and reslicing PET images. *Journal of Computer Assisted Tomography, 16,* 620–633.
Worsley, K. J., Evans, A. C., Marrett, S., & Neelin, P. (1992). A three-dimensional statistical analysis for CBF activation studies in human brain. *Journal of Cerebral Blood Flow and Metabolism, 12,* 900–918.
Worsley, K. J., Marrett, S., Neelin, P., Vandal, A. C., Friston, K. J., & Evans, A. C. (1996). A unified statistical approach for determining significant signals in images of cerebral activation. *Human Brain Mapping, 4,* 58–73.
Yan, L., Imbrosci, B., Zhang, W., Neubacher, U., Hatt, H., Eysel, U. T., et al. (2012). Changes in NMDA-receptor function in the first week following laser-induced lesions in rat visual cortex. *Cerebral Cortex, 22,* 2392–2403.
Zepeda, A., Sengpiel, F., Guagnelli, M. A., Vaca, L., & Arias, C. (2004). Functional reorganization of visual cortex maps after ischemic lesions is accompanied by changes in expression of cytoskeletal proteins and NMDA and GABA(A) receptor subunits. *Journal of Neuroscience, 24,* 1812–1821.
Zepeda, A., Vaca, L., Arias, C., & Sengpiel, F. (2003). Reorganization of visual cortical maps after focal ischemic lesions. *Journal of Cerebral Blood Flow and Metabolism, 23,* 811–820.